

Numerical Solution of the Gyroaverage Operator for the Finite Gyroradius Guiding-Center Model

Nicolas Crouseilles*, Michel Mehrenberger and Hocine Sellama

INRIA Nancy Grand-Est and IRMA, 7, rue René Descartes, 67084 Strasbourg, France.

Received 1 September 2009; Accepted (in revised version) 22 January 2010

Communicated by Zhihong Lin

Available online 15 April 2010

Abstract. In this work, we are concerned with numerical approximation of the gyroaverage operators arising in plasma physics to take into account the effects of the finite Larmor radius corrections. Several methods are proposed in the space configuration and compared to the reference spectral method. We then investigate the influence of the different approximations considering the coupling with some guiding-center models available in the literature.

PACS: 02.60.-x, 52.65.Tt, 02.70-c

Key words: Gyroaverage operator, cubic splines, Bessel function, plasma simulation, guiding-center model, Eulerian solvers for Vlasov.

1 Introduction

In strongly magnetized plasma, when collision effects are negligible, one has to deal with kinetic models since fluid models, which assume that the distribution function is close to an equilibrium, are not appropriated. However, the numerical solution of Vlasov type models is challenging since this model involves six dimensions of the phase space. Moreover, multi-scaled phenomena make the problem very difficult since numerical parameters have to solve the smallest scales. Gyrokinetic theory enables to get rid of one of these constraints since the explicit dependence on the phase angle of the Vlasov equation is removed through gyrophase averaging while gyroradius effects are retained. The so-obtained five dimensional function is coupled with the Poisson equation (or its asymptotic counterpart, the quasi-neutrality equation) which is defined on the particle coordinates. Thus solving the gyrokinetic Vlasov-Poisson system requires an operator which

*Corresponding author. *Email addresses:* crouseil@math.u-strasbg.fr (N. Crouseilles), mehrenbe@math.u-strasbg.fr (M. Mehrenberger), hocine.sellama@inria.fr (H. Sellama)

carries out from the gyrocenter to the particles coordinates. This operator is the so-called gyroaverage operator. We refer to an abundant literature around this subject (see [1,10,16] and references therein).

The present work is devoted to a numerical study of the gyroaverage operator. We intend to develop and compare different methods to deal with the numerical approximation of the gyroaverage operator.

Roughly speaking, the gyroaverage process consists in computing an average on a circle (the Larmor circle). The use of Fourier transform reduces the gyroaveraging operation by a multiplication in the Fourier space by the Bessel function. In simple geometry, this can be performed easily. However, since the Larmor radius depends also on a perpendicular velocity variable μ , the use of Fourier transform is not applicable in general geometry such as those employed in realistic tokamak equilibrium. And even in simplified circular cross-section, the Fourier approach has difficulties to deal with non-periodic boundary conditions. Several approaches have thus been developed to address these problems. Approximations of the Bessel function have been proposed such as the Padé expansion (see [7]); this approximation recovers a correct behaviour of the Bessel function for small Larmor radius and also asymptotically. Moreover, it enables to come back to the spatial configuration to take into account non-periodic boundary conditions. Other works deal with quadrature formula to evaluate the integration with respect to the gyrophase angle (see [16,17]). The so-called 4-points method is quite simple since it can be expressed into a matricial formulation. However, when the Larmor radius becomes large, the method is not very accurate since the number of quadrature points is not sufficient. Moreover, when quadrature points are different from the grid points, the authors carry out a linear interpolation from the nearby grid points of the function, which can suffer from a lack of accuracy in some cases. The method has then been extended to achieve accuracy for large Larmor radius [4,12,13]. The main improvements rely on an adaptive number of quadrature points (the number gyropoints is given by an increasing function of the gyroradius [12]), but also on a finite element formalism which enables higher order accuracy keeping the matricial formulation.

In this paper, we develop and compare methods based on the direct integration of the gyroaverage operator. First, for a fixed number of quadrature points, we compare the influence of the interpolation operator (which is of great importance when the quadrature points do not coincide with the grid points). The function is reconstructed using cubic splines polynomials to reach a good accuracy (as in [18]). However, when the number of quadrature points is fixed, it is always possible to find a Larmor radius sufficiently large so that the error becomes significant. Hence, we develop a new approach, in the same spirit as [4,12,13]; the basic point is the expansion of the function on a basis (such as polynomial basis). Computing the gyroaverage of a function then reduces to compute the gyroaverage of its basis, which are known analytically. Hence, in the same way as finite element formulation, the method can be formulated into a matricial form. The approach presents other several advantages. On the one side, the number of quadrature points is automatically determined as the intersection between the mesh and the Lar-

mor circle, which provides the necessary adaptivity to reach a good accuracy even for large Larmor circles. Contrary to previous works, the basis function are not evaluated at the quadrature points but integrated on a circle arc, which turns out to be more accurate. On the other side, the approach is quite general so that the choice of the basis is not imposed (the 4-points or N -points method can be recovered) and benefits from fast algorithms property. Indeed, when periodic boundary conditions are considered, it can be proved that the obtained matrix is circulant, which means that the matrix-vector product can be performed in a $\mathcal{O}(N \log N)$ complexity and stored in a linear cost. The present work restricts to a periodic domain in order to make comparison with spectral based method possible. It is a first step of validation which intends to carefully compare various methods of the literature and to present a general framework which includes the Bessel method and the quadrature based methods. We can extend the present periodic context to Dirichlet boundary conditions; the matrix becomes Toeplitz instead of circulant, and computations can be done with a moderate additional work. A general domain (e.g. an annulus) can then be handled by casting it in a bounding box and using an appropriate projection. For realistic geometries involving an inhomogeneous magnetic field, the situation becomes more complex, since the problem is inherently 3D, even if some approximations may lead to local 2D problems. We mention here some possible extensions which may be the purpose of further studies. On the one hand, a direct approach would be to store the full matrix which takes into account the inhomogeneous Larmor radius. The matrix should be sparse enough, since realistic Larmor radius are supposed to be small enough. On the other hand, for 2D problems, the present approach could also be used to compute a range of gyroaverages (with constant Larmor radius) and then to interpolate for evaluating the local gyroaverage.

In a second part of the paper, we are concerned with the coupling of the gyroaverage operator with the guiding-center model. This model has been introduced in [15] to take into account finite Larmor radius effect in guiding-center approximation. Many difficulties arise in this model. On the one side, the velocity drift $E \times B$ is not simple to deal with since it depends on the advected variables, and the model is not conservative when a time splitting is considered (see [2, 5]). On the other side, the gyroaverage operator also includes an integration with respect to the Larmor radius which belongs to $[0, +\infty]$. Hence a good accuracy when large Larmor radius are considered is required. But, it turns out that it is not sufficient since the numerical integration with respect to the Larmor radius is also important in order to reach a good accuracy for the gyroaverage operator. For example, traditional quadrature rules (such as trapezoidal or Laguerre ones) are not sufficiently efficient. In this context, we develop a new approach which appears to be very efficient for arbitrary wavenumbers. The coupling with the guiding-center model leads to very good results compared to the analytical results in the linear regime and to the spectral method for the gyroaverage operator.

The paper is organized as follows. First, we recall the expression of the gyroaverage operator and present the different numerical approximations that we developed. They are compared each other to an analytical solution (at least to the spectral precision). Then,

we briefly introduce the guiding-center model which takes into account of the finite Larmor radius effects before presenting the numerical results.

2 Gyroaverage operators

In this section, we introduce the notations which will be used in the rest of the paper. If we denote by $\vec{\rho} = \rho(\cos\alpha, \sin\alpha)$ with ρ the Larmor radius, the gyroaverage of a function f is

$$\mathcal{J}(f)(\vec{x}) = \frac{1}{2\pi} \int_0^{2\pi} f(\vec{x} + \vec{\rho}) d\alpha. \tag{2.1}$$

A simple way to write the operator involves the Fourier variables. Indeed, since the gyroaverage operator is a translation, it becomes a multiplication in the Fourier space

$$\begin{aligned} \mathcal{J}(f)(\vec{x}) &= \frac{1}{2\pi} \int_0^{2\pi} f(\vec{x} + \vec{\rho}) d\alpha \\ &= \frac{1}{2\pi} \int_0^{2\pi} \left[\sum_k \widehat{f}_k e^{i\vec{k}\cdot\vec{x}} e^{i\vec{k}\cdot\vec{\rho}} \right] d\alpha \\ &= \sum_k \widehat{f}_k e^{i\vec{k}\cdot\vec{x}} \left[\frac{1}{2\pi} \int_0^{2\pi} e^{i\vec{k}\cdot\vec{\rho}} d\alpha \right]. \end{aligned}$$

The integral into brackets can be expressed by the Bessel function of the first kind \mathcal{J}_0 . Indeed we have

$$\mathcal{J}_0(\rho k) = \frac{1}{2\pi} \int_0^{2\pi} e^{i\vec{k}\cdot\vec{\rho}} d\alpha = \frac{1}{2\pi} \int_0^{2\pi} e^{ik\rho\cos(\alpha-\theta)} d\alpha = \frac{1}{2\pi} \int_0^{2\pi} e^{ik\rho\cos\alpha} d\alpha,$$

where $\rho = |\vec{\rho}|$ and $k = |\vec{k}| = |k(\cos\theta, \sin\theta)|$. Hence, we conclude that

$$\widehat{\mathcal{J}(f)}(\vec{k}) = \mathcal{J}_0(\rho k) \widehat{f}(\vec{k}). \tag{2.2}$$

We are also interested in the operator including an integration with respect to the adiabatic invariant μ which, in slab geometry, quantifies the radius of the Larmor circles using $\sqrt{2\mu} = \rho$. This operator writes

$$\mathcal{I}(f)(\vec{x}) = \int_0^{+\infty} \mathcal{J}(f) \exp(-\mu) d\mu = \int_0^{+\infty} \mathcal{J}(f) \exp(-\rho^2/2) \rho d\rho. \tag{2.3}$$

This operator can be found in [15, 21] in the framework of the coupling with guiding-center type equations. One of the main difficulty we have to face with consists in an accurate approximation of the gyroaverage operator for arbitrarily large Larmor radius. A discrete integration approximation has also to be constructed to deal with the integration with respect to μ . As in the case of the gyroaverage operator \mathcal{J} , the operator \mathcal{I} has a simplified form in Fourier variables. Indeed, we have

$$\widehat{\mathcal{I}(f)}(\vec{k}) = \int_0^{+\infty} \mathcal{J}_0(k\sqrt{2\mu}) \exp(-\mu) d\mu \widehat{f}(\vec{k}) = \exp(-k^2) \widehat{f}(\vec{k}), \tag{2.4}$$

where the last equality has been obtained using the analytical result (see [6, 16]):

$$\int_0^{+\infty} \mathcal{J}_0(k\sqrt{2\mu}) \exp(-\mu) d\mu = \exp(-k^2). \tag{2.5}$$

3 Numerical approximations of the gyroaverage operators

In this section, we propose several methods for the approximation of (2.1). As a reference, we will compare the different methods to the spectral one given by (2.2). The methods can be distinguished into two classes of methods. The first one is based on approximations of the Bessel function whereas the second one intends to approximate the integral on a circle of radius ρ using different interpolation operators.

3.1 Approximation of \mathcal{J}

3.1.1 Fourier based approximations

In massively parallel gyrokinetic codes, even if spectral approaches remains difficult to manage due to the use of FFT on a large number of processors, these kinds of methods remain easy to implement. Most of the time, an approximation of the Bessel function is performed. We propose to compare two kinds approximations: the Padé (of first or second order) and Taylor expansions. Let us detail each of them in the sequel.

Padé expansion The first order Padé approximation of the Bessel function is

$$\mathcal{J}_0(k\rho) \sim \frac{1}{1+(k\rho)^2/4}. \tag{3.1}$$

whereas the second order is

$$\mathcal{J}_0(k\rho) \sim \frac{1}{1+(k\rho)^2/4-(k\rho)^4/64}. \tag{3.2}$$

The Padé approximation enables to recover the good asymptotic behaviour of the Bessel function as $\rho \rightarrow +\infty$, and it is a good approximation for small ρ . However, for intermediate Larmor radius, the Padé approximation truncates the oscillations of the Bessel function (see Fig. 1). One of the main interest of the Padé approximations is that it makes possible the computation of the gyroaverage in the real space; indeed, (3.1) is equivalent to

$$\left(1 + \frac{(k\rho)^2}{4}\right) \widehat{\mathcal{J}(f)}(\vec{k}) = \widehat{f}(\vec{k}),$$

which, using the equivalence $i\vec{k} \longleftrightarrow \nabla$, leads to the following system

$$\left(1 - \frac{\rho^2}{4} \Delta\right) \mathcal{J}(f)(\vec{x}) = f(\vec{x}). \tag{3.3}$$

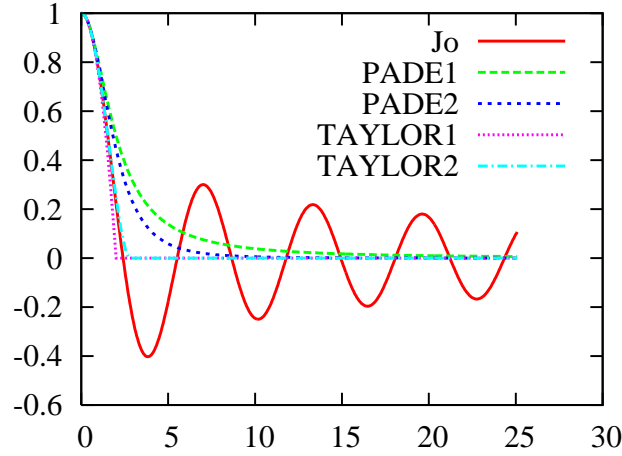


Figure 1: Different approximations in the Fourier space of the Bessel function.

The second order leads to the following equation

$$\left(1 - \frac{\rho^2}{4}\Delta + \frac{\rho^4}{64}\Delta^2\right) \mathcal{J}(f)(\vec{x}) = f(\vec{x}). \tag{3.4}$$

The gyroaverage operator appears to be a diffusion type operator. The gyroaverage function is then solution to a linear system (tridiagonal for (3.3) or pentadiagonal for (3.4) for classical spatial discretizations) in the spatial configuration.

Taylor expansion A Taylor expansion of the Bessel function is also possible. The first terms of the Taylor expansion are

$$\mathcal{J}_0(k\rho) \sim 1 - \frac{(k\rho)^2}{4} + \frac{(k\rho)^4}{64}. \tag{3.5}$$

Taylor expansions recover better the Bessel function up to $\rho < 2$, but when ρ goes to infinity, the Taylor expansions go to $-\infty$. Hence a truncation has to be performed to recover the good asymptotic behaviour (see Fig. 1) which seems difficult to express in the spatial configuration.

On Fig. 1, we compare the different approximations of the Bessel function. Computing the gyroaverage function using one of the two methods can be performed with the following algorithm:

- compute $\hat{f}(\vec{k})$ using FFT of f ;
- compute for each mode \vec{k} : $\mathcal{J}_0(k\rho)\hat{f}(\vec{k})$;
- compute $\mathcal{J}(f)(\vec{x})$ using FFT inverse of $\hat{f}(\vec{k})$.

3.1.2 Integration based method (IM)

The first step of our approach consists in expanding the function f in a basis

$$f(x_1, x_2) = \sum_{i,j} \eta_{i,j} B_i(x_1) B_j(x_2),$$

where B_i is a basis function and $\eta_{i,j}$ the associated coefficients. Hence, computing the gyroaverage of f reduces to compute the gyroaverage of the product $B_i B_j$ for all i, j :

$$\mathcal{J}(f)(x_1, x_2) = \sum_{i,j} \eta_{i,j} \mathcal{J}(B_i B_j)(x_1, x_2). \tag{3.6}$$

This formulation corresponds to a finite element method and then can be reformulated into a matricial form $\mathcal{J}(f) \approx Af$ where A is a matrix of size $N = N_{x_1} N_{x_2}$. Then, we have to compute the gyroaverage of the basis functions. Many ways can be performed to do that since we have to deal with an integration over a circle. In [17], a quadrature is performed using a 4-points method which consists in choosing 4 points equally distributed on the circle. Obviously, more points can be considered (see [4, 12]) but other strategies can also be adopted. In [17], the basis function are chosen linear, but other basis of higher degree can be used in the present formulation (quadratic splines in [4], B-splines in [12]). Note that the choice of a Fourier basis leads to the Bessel method (2.2) and thus this approach may be viewed as a general framework which makes the link between the Bessel method and quadrature based methods.

For the quadrature, several strategy can be used. Instead of a uniform quadrature, it is possible to consider each arc of the circle to compute each contribution of the integral. Since the basis is local, to compute the corresponding component of the matrix, we evaluate in each cell of the spatial mesh the quantity $\mathcal{J}_l(B_i B_j)$:

$$\mathcal{J}_l(B_i B_j)(x_1, x_2) = \frac{1}{2\pi} \int_{\alpha_l}^{\alpha_{l+1}} B_i(x_1 + \rho \cos \alpha) B_j(x_2 + \rho \sin \alpha) d\alpha. \tag{3.7}$$

We define the sequences of angles $(\alpha_l)_l$ which is the intersection of the Larmor circle of radius ρ with the mesh. This intersection is composed of points in the domain, the polar coordinates of which are (ρ, α_l) . The size of the so-obtained sequence increases as ρ increases (the number of intersection point is an increasing function of the Larmor radius, as in [12]). This enables to reach the required adaptivity to be accurate enough for large Larmor radius. Hence, the problem can be re-written as

$$\mathcal{J}(B_i B_j)(x_1, x_2) = \sum_l \mathcal{J}_l(B_i B_j)(x_1, x_2).$$

For a given basis function, this computation of $\mathcal{J}_l(B_i B_j)$ can be performed using different techniques. A simple way would be to use a quadrature formula which reduces the computation of (3.7) to an evaluation of the basis function ; for example a trapezoidal,

midpoint, Simpson or Gauss formula have been tested and the best strategy appeared to be the 3-points Gauss quadrature which leads to

$$\mathcal{J}_l(B_i B_j)(x_1, x_2) \approx \frac{1}{2\pi} \sum_k B_i(x_1 + \rho \cos \alpha_k) B_j(x_2 + \rho \sin \alpha_k) \omega_k,$$

where (α_k, ω_k) are the points and weights of the quadrature rule. Hence, according to the support of the basis function, the nearest grid points will be affected by the computation of (3.7), thanks to (3.6).

We can observe that the built matrix A has specific properties: it is possible to prove that A is block circulant. Indeed, if we denote by $\mathcal{S}_{i,j}$ the stencil of f which contributes to the computation of $\mathcal{J}(f)_{i,j}$, then the stencil $\mathcal{S}_{i+1,j}$ can easily be expressed as the shift in the i direction of $\mathcal{S}_{i,j}$. This property is sent back to the matrix which inherits the circulant property. This class of matrices has important characteristics since it is diagonalizable in the Fourier basis so that we can write [8]

$$A = PDP^*,$$

where D is a diagonal matrix and P a unitary matrix. In addition, the spectrum of A is given by the Fourier coefficients of the first line of A . Hence the diagonal matrix D can be stored into a vector, the component of which are the Fourier coefficients of the first line of A . The matrix-vector product can then be decomposed into three matrix-vector product: $p = P^* f$, $q = Dp$ and $r = Pq$. The $\mathcal{O}(N_{x_1} N_{x_2} \log N_{x_1} N_{x_2})$ complexity can be reached following the algorithm:

- compute $p = P^* f$ using FFT of f ;
- compute $q = Dp$ using $q_k = D_k p_k$;
- compute $r = Pq$ using FFT inverse of q .

Remark 3.1. As an example, if linear function together with a midpoint formula to approximate (3.7) are considered, we obtain

$$\mathcal{J}_l(B_i B_j)(x_1, x_2) \approx \frac{1}{2\pi} B_i(x_1 + \rho \cos \alpha_{l+1/2}) B_j(x_2 + \rho \sin \alpha_{l+1/2}).$$

If we denote by m, n the index such that $(x_1 + \rho \cos \alpha_{l+1/2}, x_2 + \rho \sin \alpha_{l+1/2}) \in [x_{1,m}, x_{2,n}, x_{1,m+1}, x_{2,n+1}]$, the contributed values of $\mathcal{J}_l(f)(x_1, x_2)$ are $f_{m,n}, f_{m+1,n}, f_{m,n+1}, f_{m+1,n+1}$. More complex formulae can be derived for the cubic splines basis functions since the support is equal to 16 cells in two dimensions. Following the example of linear basis functions, we get for the matrix A

$$A = \begin{pmatrix} A_0 & A_1 & \dots & \dots & A_{N-1} \\ A_{N-1} & A_0 & A_1 & \dots & A_{N-2} \\ A_{N-2} & A_{N-1} & A_0 & \dots & A_{N-3} \\ \vdots & \ddots & \ddots & \ddots & \vdots \\ A_1 & A_2 & \dots & A_{N-1} & A_0 \end{pmatrix}, \tag{3.8}$$

where each A_k matrix is a circulant matrix of the form

$$A_k = \begin{pmatrix} a_{k,0} & a_{k,1} & \dots & \dots & a_{k,N-1} \\ a_{k,N-1} & a_{k,0} & a_{k,1} & \dots & a_{k,N-2} \\ a_{k,N-2} & a_{k,N-1} & a_{k,0} & \dots & a_{k,N-3} \\ \vdots & \ddots & \ddots & \ddots & \vdots \\ a_{k,1} & a_{k,2} & \dots & a_{k,N-1} & a_{k,0} \end{pmatrix}.$$

We detail the algorithm of this approach in the simplest case of a linear basis and a mid-point quadrature formula.

Algorithm 3.1:

Step 1. Computation of the sequence $(\alpha_l)_l$ defined as the intersection between the Larmor circle and the mesh.

Step 2. Initialization $a_{m,n} = 0$.

Step 3. For each l , search for (m,n) such that $(x_1 + \rho \cos \alpha_{l+1/2}, x_2 + \rho \sin \alpha_{l+1/2}) \in [x_{1,m}, x_{2,n}, x_{1,m+1}, x_{2,n+1}]$, with $\alpha_{l+1/2} = (\alpha_l + \alpha_{l+1})/2$.

Let us denote by $\beta_1 = (x_1 + \rho \cos \alpha_{l+1/2} - x_{1,m})$ and $\beta_2 = (x_2 + \rho \sin \alpha_{l+1/2} - x_{2,n})$. Then, with $\Delta \alpha_l = (\alpha_{l+1} - \alpha_l)/2\pi$, we update

$$\begin{aligned} a_{m,n} &\leftarrow a_{m,n} + (\Delta x_1 - \beta_1)(\Delta x_2 - \beta_2)\Delta \alpha_l, \\ a_{m+1,n} &\leftarrow a_{m+1,n} + \beta_1(\Delta x_2 - \beta_2)\Delta \alpha_l, \\ a_{m+1,n+1} &\leftarrow a_{m+1,n+1} + \beta_1\beta_2\Delta \alpha_l, \\ a_{m,n+1} &\leftarrow a_{m,n+1} + (\Delta x_1 - \beta_1)\beta_2\Delta \alpha_l, \end{aligned}$$

where $\Delta x_{1,2}$ is the size of the mesh in the $x_{1,2}$ -directions.

This last step has to be performed for each quadrature points when other quadratures are employed. Note that in the cubic splines case, the coefficients η are linked to the pointwise values of f by a matricial relation $C\eta = f$. Hence, thanks to the previously derived formula $A\eta = \mathcal{J}(f)$, we have the matricial system $AC^{-1}f = \mathcal{J}(f)$. Since the product of two circulant matrices is also circulant, the previous algorithm is always available.

3.2 Comparison of the different numerical approximations

This section is devoted to a numerical comparison of the different methods presented above. On the one side, we look at the Fourier based methods (PADE1 (3.1), PADE2 (3.2), TAYLOR1 and TAYLOR2 (3.5)) and on the other side, we are interested in integration based methods. At first, standard quadrature based methods are investigated using cubic splines (SPL) or linear splines (LIN) for different numbers of uniform quadrature points (4,8 and 16). The number of quadrature points is mentioned as a suffix of the corresponding method. Then we consider the adaptive integration method (IM) either for linear (IM-LIN) or cubic splines (IM-SPL).

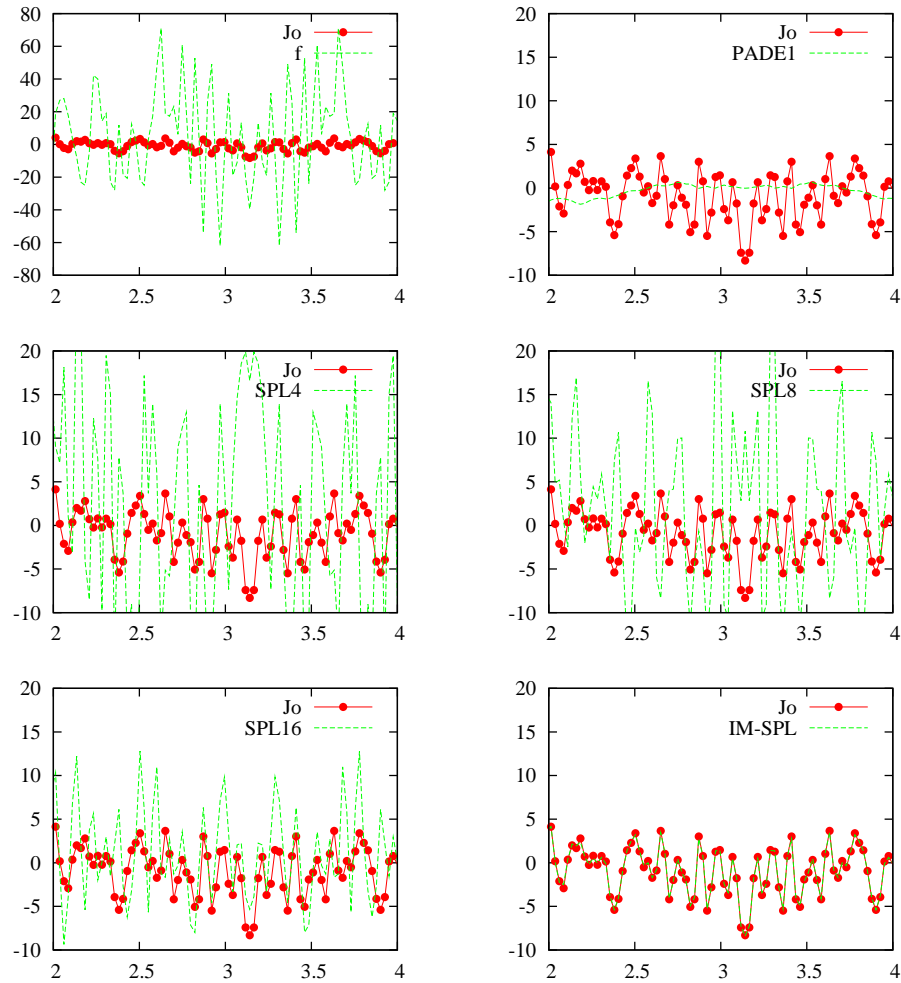


Figure 2: Gyroaverage function as a function of x , evaluated at $y = \pi/2$. Comparison of the different methods. $\rho = 0.5$.

The following analytical function is considered

$$f(x_1, x_2) = \sum_{k_1=1}^M \sum_{k_2=1}^M \beta_{k_1, k_2} \cos(k_1 x_1) \cos(k_2 x_2), \quad (x_1, x_2) \in [0, 2\pi]^2, \quad (3.9)$$

where β_{k_1, k_2} is a random value between -1 and 1 .

Since the Bessel function is tabulated, we will consider as the reference solution the solution given by (2.2). Hence, we consider the error made by the different methods with respect to the reference solution. The number of points used to sample the analytical function is $N = 256$ in each direction. On Fig. 2, we plot the function $f(x, y = \pi/2)$ (given by (3.9) and the corresponding gyroaverage function $\mathcal{J}(f)(x, y = \pi/2)$ for all $x \in [0, 2\pi]$,

with a Larmor radius $\rho=0.5$. We can observe the influence of the gyroaverage operator: each small scale is damped. We also observe the different approximations: the Padé approximation over-damps small scales whereas the N -points methods (with $N=4,8,16$) with cubic B-splines interpolation operator do not damp enough small structures even if the choice of $N=16$ points leads to quite good results. The IM approach is very close to the reference solution.

On Figs. 3 and 4, we plot the L^1 error between the reference solution (given by the Bessel approach) and the different methods as a function of ρ (normalized to $\Delta x/4$, with Δx the size of the mesh) for the different methods. The results of the IM (i.e. IM-LIN and IM-SPL) approach are shown on Fig. 4 (right).

First, we observe that only the IM method is able to keep accuracy for large Larmor radius since the method with a fixed number of quadrature points fails when ρ becomes sufficiently large. Moreover, we can see a gap between linear and cubic splines based methods; as expected, cubic splines produce a very low error. This small error can be reached by the linear approach with four points when ρ is proportional to the mesh size. In this case, LIN4 and SPL4 are equivalent since there is no interpolation error. The same remark is available for IM. For Fourier based methods, even if the Taylor expansion gives very good results for $\rho \leq 2$, the other methods (Padé) lead to an important error compared to SPL16 which is plotted as a reference on Fig. 3.

Another diagnostic can be plotted for this example. Indeed, thanks to the equality (2.2), for a given mode \vec{k} such that $\hat{f}(\vec{k}) \neq 0$, we can consider the Fourier transform of the gyroaverage function divided by the Fourier transform of the function. This quantity can be viewed as an approximation of the Bessel function \mathcal{J}_0

$$\frac{\widehat{\mathcal{J}(f)}(\vec{k})}{\hat{f}(\vec{k})} \approx \mathcal{J}_0(\rho k).$$

Considering different values of ρ leads to Figs. 5 and 6. The same conclusions as before arise since the integration based methods become less accurate as ρ increases. Even if a good accuracy can be reached by adding quadrature points, it is always possible to find $k\rho$ (which can be arbitrarily large), such that the method fails. On the contrary, IM with a non-uniform quadrature (see Fig. 6), provides a very good accuracy for both basis function (linear and cubic splines) even for very large Larmor radius. Nevertheless, as observed in the previous figures, the two basis functions give rise to different results. Fig. 6 on the right presents the difference between the Bessel function and the IM methods. We clearly observe one order of difference between the use of linear and cubic B-splines. The same is true for Fig. 7, in which we made a zoom for small radius to distinguish linear and cubic spline approximations. We can observe a lack of accuracy of the linear based method compared to the cubic splines approach. The difference is about 1% whereas the cubic splines approach is about two orders more accurate and motivate the use of cubic spline basis functions. Obviously, the storage of the matrix requires more computations when cubic B-splines are used instead of a linear basis. But one has to point out that the matrix has to be calculated just once at the beginning of a dynamical simulation.

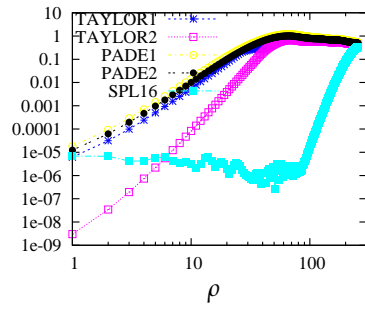


Figure 3: For Fourier based method, L^1 error in logscale between the Bessel approach as a function of the Larmor radius ρ . The method SPL16 is plotted for comparison.

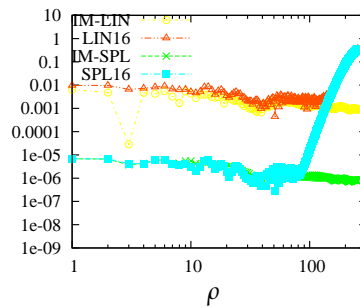
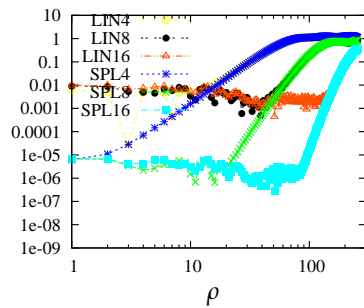


Figure 4: For the integration methods, L^1 error in logscale between the Bessel approach as a function of the Larmor radius ρ . When the number of quadrature points is referred, the uniform quadrature is used. When it is not referred, the non-uniform quadrature is employed.

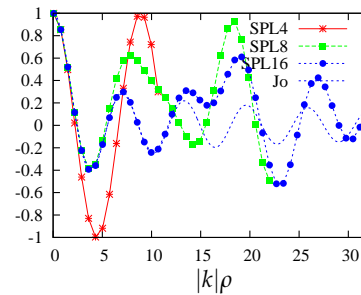
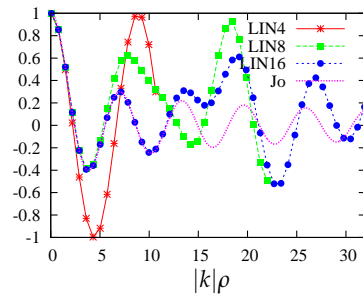


Figure 5: Approximated Bessel function as a function of $k\rho$. Comparison between the IM using linear basis (left) and cubic splines basis (right) in the uniform quadrature case. Study of the influence of the number of quadrature points.

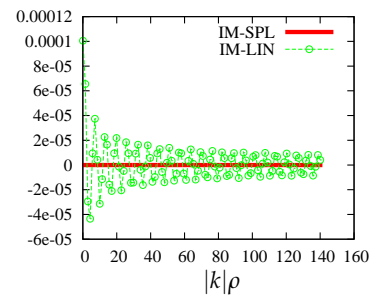
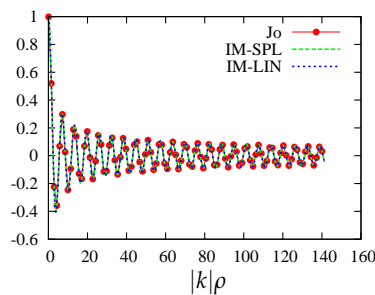


Figure 6: Approximated Bessel function as a function of $k\rho$. Comparison between the IM approach using linear or cubic splines basis (left) and error between IM and the Bessel function for linear or cubic splines basis (right). Non-uniform quadrature case.

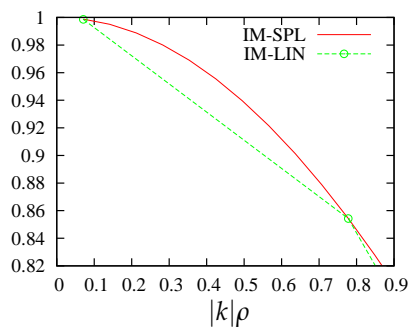


Figure 7: Approximated Bessel function as a function of $k\rho$. Comparison between IM using linear and cubic splines basis functions.

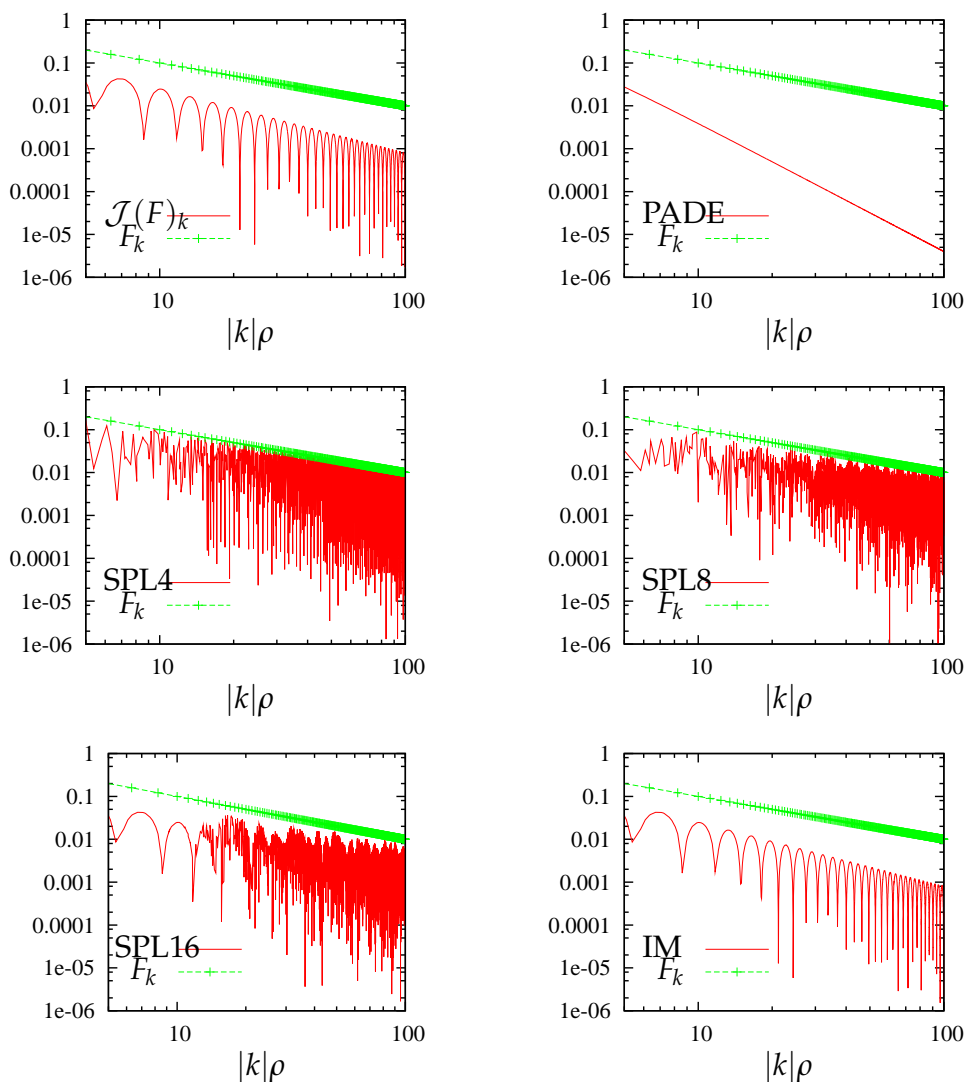


Figure 8: Comparison of the gyroaverage function and the function in the Fourier space. Comparison of the different methods. $\rho=1$.

Finally, on Fig. 8, we investigate the effect of the gyroaverage operator on high wavenumbers (see [19]). Considering a bath of modes (like (3.9), with $M = 100$ and with the β_{k_1, k_2} coefficients which are proportional to $1/k^2$), we investigate the influence of the different approximations of the gyroaverage operator on the high wavenumbers (since all the methods are more or less accurate for low wavenumbers). The Bessel function $\mathcal{J}_0(k)$ is equivalent to $1/\sqrt{k}$ when $k \rightarrow \infty$ so that the coefficients will be equivalent to $1/k^{3/2}$ for large values of k . The Padé approximant is in $1/k^2$ so that the high wavenumbers are strongly damped since they behave in $1/k^4$ for large k . The N -points methods (for $N = 4, 8, 16$) are not very accurate for large wavenumbers (as already observed previously) since the asymptotic behaviour is nearly superimposed with this of the function. On the contrary, the IM method presents a very good asymptotic behaviour, very close to the Bessel method one.

3.3 Approximation of \mathcal{I}

This subsection is devoted to the study of the gyroaverage operator integrated with respect to $\mu = \rho^2/2$. This operator intervenes in the model (4.1)-(4.2) and justifies the search of accurate methods to approximate the gyroaverage operator for large Larmor radius. The only thing to do consists in looking for a precise numerical integration with respect to μ . However, we will see that it is not so easy to derive a numerical integration which is accurate for arbitrarily large wavenumbers. We first extend IM in a simple way before presenting a new approach. The numerical results will be compared to analytical results given by the following equality (see [6])

$$\int \mathcal{J}_0(\rho k) \exp(-\mu) d\mu = \exp(-k^2), \quad \text{with } \rho = \sqrt{2\mu}. \tag{3.10}$$

3.3.1 Extension of IM

This subsection intends to extend in a classical way the IM approach to approximate the \mathcal{I} operator. To do that, we apply the Laguerre quadrature to the previous IM approach. The main advantage of the IM approach is that the integration with respect to μ can be stored once for all into the matrix A since

$$\int \mathcal{J}(f) \exp(-\mu) d\mu \approx \sum_{l=0}^{N-1} A_l f \omega_l = \left(\sum_{l=0}^{N-1} A_l \omega_l \right) f = Af.$$

Thanks to the circulant property of each matrix A_l , we can deduce that the linear combination of circulant matrix is also circulant so that fast algorithm can always be used.

3.3.2 Integration based method IM_μ

As an extension of the IM method developed above for the operator \mathcal{J} , this subsection is devoted to the presentation of a new approach in the spirit of the method presented in

Subsection 3.1.2. Indeed, the first step also consists in the expansion of the f in a basis. Then, the operator \mathcal{I} has to be applied to the basis functions:

$$\mathcal{I}(f)(x_1, x_2) = \sum_{i,j} \eta_{i,j} \mathcal{I}(B_i B_j)(x_1, x_2). \tag{3.11}$$

As remarked previously, the value of $\mathcal{I}(f)$ at one grid point can be deduced from the value of $\mathcal{J}(f)(0,0)$ thanks to a shifting procedure, so that we can write

$$\begin{aligned} \mathcal{I}(f)(0,0) &= \frac{1}{2\pi} \int_0^{+\infty} \int_0^{2\pi} f(\rho \cos \alpha, \rho \sin \alpha) \exp(-\rho^2/2) \rho d\rho d\alpha \\ &= \frac{1}{2\pi} \sum_{i,j} \eta_{i,j} \int_0^{+\infty} \int_0^{2\pi} B_i(\rho \cos \alpha) B_j(\rho \sin \alpha) \exp(-\rho^2/2) \rho d\rho d\alpha \\ &= \frac{1}{2\pi} \sum_{i,j} \eta_{i,j} \int \int_{\mathbb{R}^2} B_i(x_1) B_j(x_2) \exp(-(x_1^2 + x_2^2)/2) dx_1 dx_2 \\ &= \frac{1}{2\pi} \sum_{i,j} \eta_{i,j} \int_{\mathbb{R}} B_i(x_1) \exp(-x_1^2/2) dx_1 \int_{\mathbb{R}} B_j(x_2) \exp(-x_2^2/2) dx_2. \end{aligned}$$

Due to the finite size of the support of the chosen basis function (cubic B-splines in our case), the integrations arising in the last formula can be performed using formal computations. Indeed, in our periodic configuration, the integral we have to deal with writes

$$\begin{aligned} \int_{\mathbb{R}} B_i(x_1) \exp(-x_1^2/2) dx_1 &= \int_{\mathbb{R}} B\left(\frac{x_1 - x_i}{\Delta x}\right) \exp(-x_1^2/2) dx_1 \\ &= \int_{\mathbb{R}} B(x_1) \exp(-(\Delta x x_1 + x_i)^2/2) dx_1 \\ &= \int_{\mathbb{R}} B(x_1) \exp(-\Delta x(x_1 + i))^2/2) dx_1 \quad \text{with } x_i = i\Delta x \\ &= \int_{-2}^1 B(x_1) \sum_{k=-\infty}^{+\infty} \exp(-\Delta x(x_1 + i) + 2\pi k)^2/2) dx_1, \end{aligned}$$

where the B-spline is given by

$$6B(x_1) = \begin{cases} (2 - |x_1|)^3 & \text{if } 1 \leq |x_1| \leq 2, \\ 4 - 6x_1^2 + 3|x_1|^3 & \text{if } 0 \leq |x_1| \leq 1, \\ 0 & \text{otherwise.} \end{cases}$$

Hence we have to pre-compute the quantity

$$A_i = \int_{-2}^1 B(x_1) \sum_{k=-\infty}^{+\infty} \exp(-\Delta x(x_1 + i) + 2\pi k)^2/2) dx_1.$$

Obviously the infinite sum can be truncated since for sufficiently large value of k , the term $\exp(-\Delta x(x_1+i)+2\pi k)^2/2)$ becomes negligible. Hence, it leads to the following expression of the approximation of the operator \mathcal{I}

$$\mathcal{I}(f)(0,0) = \sum_{i,j} \eta_{i,j} A_i A_j. \tag{3.12}$$

To recover the value of $\mathcal{I}(f)$ at another grid point, a shift has to be performed. This property can be summarized by

$$\mathcal{I}(f)(x_1, x_2) \approx Af,$$

where A is a block-circulant matrix of type (3.8) which can be stored in a $\mathcal{O}(N_1 N_2)$ cost whereas the matrix-vector product can be performed with $\mathcal{O}(N_1 N_2) \log(N_1 N_2)$ complexity.

Remark 3.2. The sum of the A_i coefficient can be analytically computed

$$\begin{aligned} \sum_{i=0}^{N_1-1} A_i &= \sum_{i=0}^{N_1-1} \int_{-2}^1 B(x_1) \sum_{k=-\infty}^{+\infty} \exp(-\Delta x(x_1+i)+2\pi k)^2/2) dx_1 \\ &= 1/\sqrt{2\pi}. \end{aligned}$$

3.3.3 Numerical results

In this part, we intend to compare the two methods introduced above for the approximation of the operator \mathcal{I} defined by (2.5).

The following numerical results present the comparison between the analytical solution (given by (3.10)) and the approximated ones, given by the IM and IM μ approaches. We consider on Fig. 9 the error in the Fourier space. For different values of k , we plot the error between the two methods and the analytical value $\exp(-k^2/2)$. We can observe that the Laguerre quadrature gives random type results in which it is difficult to be confident. On the contrary IM μ is accurate independently of k . This is confirmed by Fig. 10 in which we plot $\mathcal{I}(f)(x, y = \pi/2)$, for all $x \in [0, 2\pi]$. We can observe that fast oscillations are not damped by the Laguerre quadrature whereas IM μ leads to smooth results which is in a good accordance with the fact that high modes are strongly damped by a coefficient equal to $\exp(-k^2/2)$.

Even if we conclude on the very good behaviour of IM for large Larmor radius in the previous section, it is not sufficient for the operator \mathcal{I} . This is due to the fact that we have to integrate an oscillating function, in which the oscillations depends on the excited modes: the more k is important, the more the function oscillates (see Fig. 11). The integration of oscillating function is not trivial and classical quadratures like Laguerre quadrature is not able to accurately capture the oscillations of the integrand. Moreover, one other difficulty comes from time dependent problems in which it is difficult to control the excited modes. It is important to develop a method that is precise independently

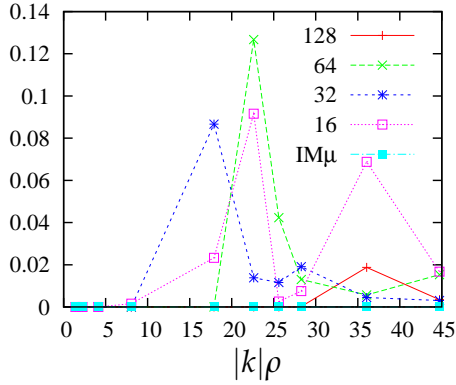


Figure 9: Error between $\int_0^{+\infty} \mathcal{J}_0(k\sqrt{2\mu})\exp(-\mu)d\mu$ as a function of $k\rho$ for the extension of IM with a different number of Laguerre points and for $IM\mu$.

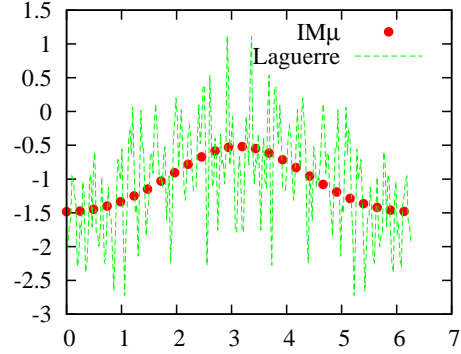


Figure 10: $\mathcal{I}(f)(x, \pi/2)$ as a function of $x \in [0, 2\pi]$. Comparison of the extension of IM (128 Laguerre points are used) with $IM\mu$. f is a bath of modes, with higher modes equal to (100,100).

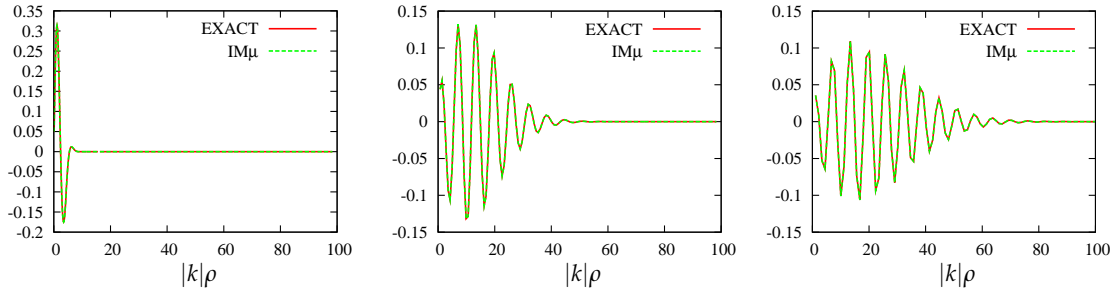


Figure 11: $\mathcal{J}_0(k\rho)\exp(-\mu)$ as a function of $k\rho$ for three different modes (1,2), (10,10) and (20,10). $IM\mu$ is also plotted.

of the oscillating character of the integrated function, in other words, for arbitrarily values of k . In the present context, $IM\mu$ is very efficient and extensions of the approach to the computation of the density $n(\vec{x}) = \int_0^{+\infty} \mathcal{J}(f)(\vec{x}, \mu)d\mu$ in gyrokinetic code is currently investigated.

4 Guiding-center simulation with finite Larmor radius effects

This section is devoted to the coupling of the gyroaverage operator with the guiding-center model. This model has been introduced in [15] and simulations have been performed in [9, 11, 14, 22]. This model considers the evolution of the guiding-center density $f = f(t, x_1, x_2)$ in the poloidal plan of the tokamak (see Appendix A for more details on its derivation)

$$\partial_t f + \nabla \cdot (\bar{v}_D f) = 0, \quad \bar{v}_D = e_z \times \nabla \mathcal{I}(\Phi), \tag{4.1}$$

coupled with the Poisson equation for the electric potential Φ

$$-\Delta\Phi = \mathcal{I}(f), \tag{4.2}$$

supplemented with an initial condition: $f(0, \vec{x}) = f_0(\vec{x})$. The expression of the operator \mathcal{I} is given by (2.3).

Several studies can be found concerning the model (4.1)-(4.2) but gyroradius effects are often left untreated [2, 21, 24]. In this simplified context, the instability growth rate which quantifies the departure of the unknown from an equilibrium can be computed in a certain range of wavenumber (see [21]). The computations of [21] can be generalized for every wavenumber by looking for imaginary part of eigenvalues. These computations are detailed in Appendix B. Nevertheless, the extension of this strategy to the gyroradius case (4.1)-(4.2) seems to be difficult and only few numerical results are available in the literature (see however [11, 14, 22]).

4.1 Numerical results

We perform simulations of the model (4.1)-(4.2) coupled with the gyroaverage operator \mathcal{I} . One of our main goal is to observe the influence of the gyroaverage operator \mathcal{I} on the dynamics of f . To that purpose, periodic conditions are considered in both spatial directions x_1 and x_2 , and the initial condition is (see [21] and Appendix B)

$$f(t=0, x_1, x_2) = \sin(x_1) + \epsilon \cos(kx_2), \quad (x_1, x_2) \in [0, 2\pi] \times [0, 2\pi/k].$$

As mentioned above, when the gyroaverage operator is neglected, it is possible to compute the instability growth rate for a given k (see Appendix B). However, it seems difficult to extend these computations to the finite Larmor radius case. We can however deduce a qualitative behaviour to anticipate the numerical results: indeed, since the gyroaverage operator can be approximated at the first order by a diffusion operator, we expect that the obtained instability growth rates will be lower to the zero-Larmor radius case. We can also compare the developed method to the one expressed in Fourier variables through (2.4). It provides us a reference solution for \mathcal{I} that will be compared to the $IM\mu$ approach.

The numerical solution of the guiding-center model is performed using a conservative semi-Lagrangian method (see [2] for more details). The time step is equal to $\Delta t = 0.1$, and the number of points is equal to 128 in each direction. The $IM\mu$ approach is used to deal with the operator \mathcal{I} . The reference solution (called EXACT in the numerical results) will be given by formula (2.4) for the gyroaverage step.

We are interested in the following diagnostics. Since the enstrophy $\|f(t)\|_{L^2}$

$$\mathcal{E}_f(t) = \int |f(t, x_1, x_2)|^2 dx_1 dx_2, \tag{4.3}$$

is preserved with time, this quantity is a good information to test the quality of our results for long time simulations. We are also interested in the time evolution of the Fourier modes of Φ for which we expect a exponential growth rate.

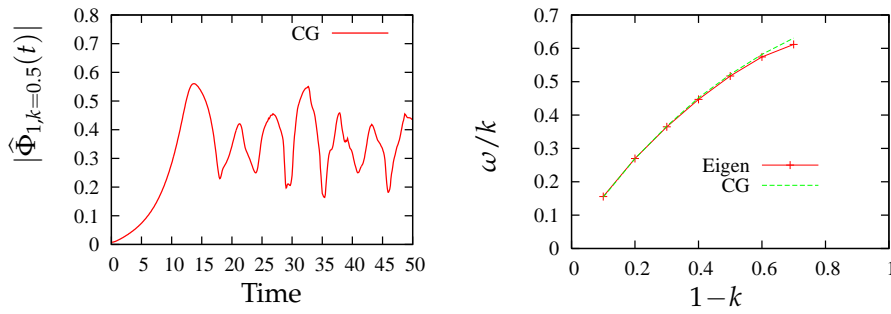


Figure 12: Left: first Fourier mode of the electric potential for $k=0.5$ as a function of time. Right: Instability growth rate divided by k as a function of $(1-k)$ in the case without Larmor radius. Eigen corresponds to the maximum imaginary part of the eigenvalues of the linearized system (see Subsection B.2) divided by k and CG corresponds to the numerical result obtained using PSM.

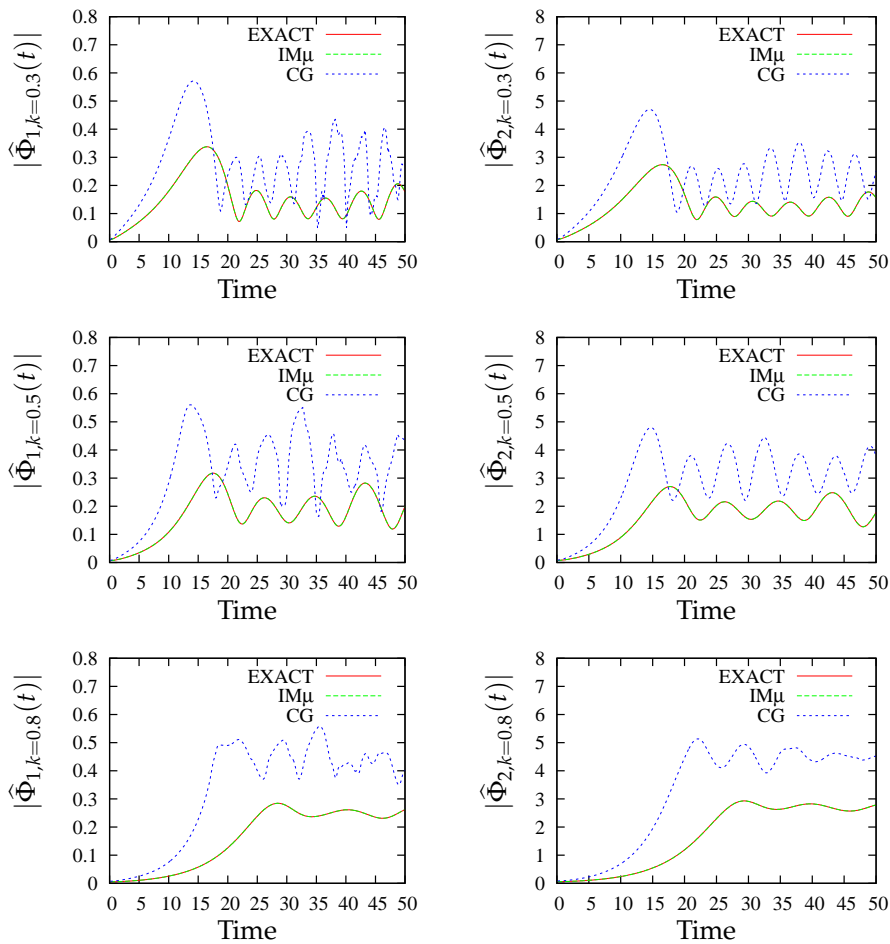


Figure 13: First Fourier mode $|\hat{\Phi}_{1,k}(t)|$ (left column) and second Fourier mode $|\hat{\Phi}_{2,k}(t)|$ (right column) of the electric potential as a function of time for $k=0.3,0.5,0.8$. Comparison between the zero Larmor radius case (CG) and the Larmor radius case (for IM μ and EXACT method).

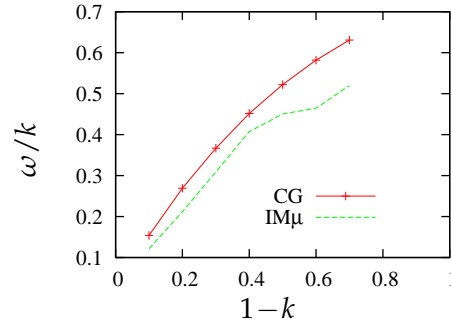


Figure 14: Normalized instability growth rate ω/k as a function of $(1-k)$ in the case without Larmor radius (CG) and with Larmor radius effects (IM μ).

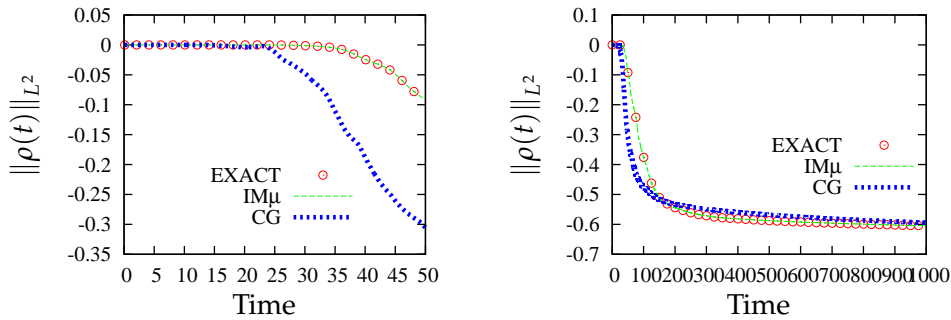


Figure 15: Time evolution of the L^2 norm of the density. Comparison between the zero Larmor radius case (CG) and the Larmor radius case (for IM μ and EXACT method). The left figure is a zoom of the right one.

On Fig. 12, we first plot the result obtained by the PSM method (Parabolic Splines Method, see [2, 25]) for the guiding-center model without gyroaverage operator (zero Larmor radius case). The PSM method enables to solve 1D conservative transport problems, which provides a useful tool for multi-dimensional problems when we deal with splitting procedure. As an example of the precision of this approach, we can notice the good agreement concerning the growth rate instability between the *a priori* computed ones (see Appendix B) and the growth rate given by the code. Good conservation properties are also observed for non linear long time simulations (see [2]). Then, in the sequel, we compare and analyse the guiding-center model with gyroaverage operator (4.1)-(4.2). On Fig. 13, we plot the first and second Fourier modes of the electric potential $|\widehat{\Phi}_{1,k}(t)|$ and $|\widehat{\Phi}_{2,k}(t)|$ as a function of time. We observe the influence of the operator \mathcal{I} on the modes of the electric potential. Indeed, the growth rate is clearly lower than in the zero Larmor radius case. We also observe the very good agreement between the EXACT curve and the results given by the IM μ method, even after the linear phase (which occurs up to $t \approx 25 \omega_p^{-1}$). These observations are summarized on Fig. 14, in which we plot the instability growth rate normalized to the wavenumber as a function to $(1-k)$ (like in [2, 21]). Different simulations have been performed by making k varying from 0.1 to 0.7; we then compute the linear growth rate and compare to the zero Larmor radius case. We can

Table 1: Comparison of the CPU time of the different method for the coupling with the guiding-center model. 500 iterations.

	CG	EXACT	IM μ
64 \times 64	2min. 10s.	2min. 40s.	2min. 40s.
128 \times 128	10min.30s.	13min.	13min.

observe the influence of the operator \mathcal{I} on the instability growth rate. As expected, the growth rates are lower when finite Larmor radius effects are considered. We can also remark the good behavior of the IM μ method since the results of the analytical computation of the gyroaverage operator are very well recovered. We are also interested on Fig. 15 in the time evolution of the L^2 norm (4.3). We remark that this quantity is very well conserved, in a best way as when gyroradius effects are neglected. This can be explained by the regularization effect of the gyroaverage operator. Hence, fine structures which develop are removed by the gyroaverage operator before becoming lower to the mesh size. However, for large time, the asymptotic behaviour seems very similar. Finally, we mention on Table 1 a small comparison of the computational cost of the different approaches. When the matrix involved in the IM μ approach is stored once for all, the computational cost is very similar to that of the analytical method; indeed, the additional cost compared to the zero Larmor radius case is essentially due to the use of FFT in both cases.

5 Conclusion

In this work we developed different methods for the approximation of gyroaverage operators arising in gyrokinetic models. We compare the methods existing in the literature and observe that a fixed number of quadrature points cannot be accurate for large Larmor radius. Moreover, the developed method IM is shown to be very accurate, can be run using fast algorithms and is low storage. The extended IM μ approach has been proven to be very accurate when the integration with respect to the adiabatic invariant is considered, assuming an exponential profile of the distribution function in the μ direction. The coupling with the guiding-center model confirms these observations.

We are currently thinking about several extensions applied to the quasi-neutrality equation. The present approach enables a matrix formulation of the quasi-neutrality equation in the spirit of [17]. Indeed, the quasi-neutrality equation involves the gyroaverage operator \mathcal{J}_μ which is applied twice to the electric potential (see [16, 17]) and once to the distribution function. This will make the object of a future work.

Appendix A

We consider the drift-diffusion model in slab for the ions satisfied by the distribution function $f(t, x_1, x_2, z, v_z, \mu)$

$$\partial_t f + v_D \cdot \nabla_x f + v_z \partial_z f - \mathcal{J}(E_z) \partial_{v_z} f = 0, \tag{A.1}$$

where $v_D = \mathcal{J}(E) \times e_z$ and with the Poisson equation

$$\nabla \cdot E = \int \mathcal{J}(f) dv_z d\mu - n_e.$$

If we assume f is periodic in the z direction, the integration of (A.1) with respect to z and v_{\parallel} leads to

$$\partial_t g + v_D \cdot \nabla_x g = 0, \quad \text{with } g = g(t, x, \mu). \tag{A.2}$$

If we now assume that the μ profile of g is Maxwellian so that

$$g(t, x, \mu) = n(t, x) \exp(-\mu),$$

we obtain, after integration of (A.2) with respect of μ

$$\partial_t n + \tilde{v}_D \cdot \nabla_x n = 0, \quad \text{with } \tilde{v}_D = \int_0^{+\infty} \mathcal{J}(E) \exp(-\mu) d\mu \times e_z. \tag{A.3}$$

The Poisson equation then writes

$$\nabla \cdot E = \int_0^{+\infty} \mathcal{J}(n) \exp(-\mu) d\mu - n_e.$$

The electron can be modeled through the equation as (A.3) since the $E \times e_z$ drift is independent of the mass of the particles. Considering the total charge as unknown leads to

$$\partial_t n + (\mathcal{I}(E) \times e_z) \cdot \nabla_x n = 0, \quad \text{with } \nabla \cdot E = \mathcal{I}(n).$$

Appendix B

In this subsection, we detail the computations to derive a dispersion relation. The first part try to re-write the computations of [22] whereas in a second time a discrete dispersion relation is derived.

B.1 Analytical computation

Following [22], we linearize the guiding-center model (without gyroaverage operator) around an equilibrium state $(n_0(x), \Phi_0(x))$ to obtain

$$\partial_t n_1 - \partial_y \Phi_1 \partial_x n_0 + \partial_x \Phi_0 \partial_y n_1 = 0, \quad -\Delta \Phi_1 = n_1.$$

where $n_0(x)$ and $\Phi_0(x)$ are coupled by

$$\partial_x^2 \Phi_0(x) = -n_0(x).$$

Considering Laplace transform in t and Fourier transform in the y variable leads to

$$-i\omega n_1 - ik_y \Phi_1 \partial_x n_0 + ik_y n_1 \partial_x \Phi_0 = 0, \quad (\text{B.1})$$

where n_1 and Φ_1 denote now the Laplace and Fourier transforms of respectively n_1 and Φ_1 . The same operations applied to the Poisson equation give

$$(-\partial_x^2 + k_y^2) \Phi_1 = n_1. \quad (\text{B.2})$$

Hence, by replacing n_1 in (B.1) by its expression given by (B.2), we can derive after few algebra an differential equation satisfied by Φ_1 (the Rayleigh equation):

$$(v_0 - c)(\partial_x^2 \Phi_1 - k_y^2 \Phi_1) - \Phi_1 \partial_x^2 v_0 = 0, \quad (\text{B.3})$$

or

$$\partial_x^2 \Phi_1 - \frac{\partial_x^2 v_0}{(v_0 - c)} \Phi_1 - k_y^2 \Phi_1 = 0, \quad (\text{B.4})$$

with $c = \omega/k_y$ and $v_0 = \partial_x \Phi_0$ is the drift vorticity. Following the computations of [21], we assume inflexion points at $x = x_s$. To find unstable solution for (B.4), we first have to find stable neutral solution from which unstable solution can then be constructed as $c \rightarrow v_s = v_0(x_s)$ or $(\text{Im}(c) \rightarrow 0)$. Now, the neutral stable solution Φ_s can be obtained by replacing in (B.3) $c = v_0(x_s) = v_s$ and $k_y = k_{y_s}$ to obtain

$$(v_0 - v_s)(\partial_x^2 \psi_s - k_{y_s}^2 \psi_s) - \partial_x^2 v_0 \psi_s = 0, \quad (\text{B.5})$$

or, in the form of (B.4)

$$\partial_x^2 \psi_s - \frac{\partial_x^2 v_0}{(v_0 - v_s)} \psi_s - k_{y_s}^2 \psi_s = 0. \quad (\text{B.6})$$

We now consider the difference between (B.4) multiplied by ψ_s and (B.6) multiplied by ψ to obtain

$$\partial_x (\psi_s \partial_x \Phi_1 - \Phi_1 \partial_x \psi_s) - (k_y^2 - k_{y_s}^2) \Phi_1 \psi_s - \partial_x^2 v_0 \left(\frac{1}{v_0 - c} - \frac{1}{v_0 - v_s} \right) \Phi_1 \psi_s = 0.$$

Integrating between x_1 and x_2 we get (with periodic boundary conditions)

$$\int_{x_1}^{x_2} \Phi_1 \psi_s dx = \frac{c - v_s}{k_y^2 - k_{y_s}^2} \int_{x_1}^{x_2} \frac{\partial_x^2 v_0 \Phi_1 \psi_s}{(v_0 - c)(v_0 - v_s)} dx. \quad (\text{B.7})$$

In order to find unstable solutions (such that $Im(c) > 0$) close to the neutral solution, we study the limit in (B.7) as $c \rightarrow v_s$ ($c_i \rightarrow 0, k_y \rightarrow k_{ys}, \Phi_1 \rightarrow \psi_s$), to get

$$\begin{aligned} \int_{x_1}^{x_2} \psi_s^2 dx &= \left(\frac{dc}{dk_y^2} \right)_{k_y^2=k_{ys}^2} \lim_{c \rightarrow v_s} \int_{x_1}^{x_2} \frac{\partial_x^2 v_0 \Phi_1 \psi_s}{(v_0 - c)(v_0 - v_s)} dx \\ &= \left(\frac{dc}{dk_y^2} \right)_{k_y^2=k_{ys}^2} \left[\lim_{c \rightarrow v_s} \int_{x_1}^{x_2} \frac{(v_0 - Re(c))}{(v_0 - Re(c))^2 + Im(c)^2} \frac{\partial_x^2 v_0 \Phi_1 \psi_s}{(v_0 - v_s)} dx \right. \\ &\quad \left. + i \lim_{c \rightarrow v_s} \int_{x_1}^{x_2} \frac{Im(c)}{(v_0 - Re(c))^2 + Im(c)^2} \cdot \frac{\partial_x^2 v_0 \cdot \psi \psi_s}{(v_0 - v_s)} dx \right]. \end{aligned}$$

We then recover the formula of [21]

$$\begin{aligned} \int_{x_1}^{x_2} \psi_s^2 dx &= \left(\frac{dc}{dk_y^2} \right)_{k_y^2=k_{ys}^2} \left[P \int_{x_1}^{x_2} \frac{\partial_x^2 v_0 \psi_s^2}{(v_0 - v_s)^2} dx \right. \\ &\quad \left. + i \lim_{c \rightarrow v_s} \int_{x_1}^{x_2} \frac{Im(c)}{(v_0 - Re(c))^2 + Im(c)^2} \frac{\partial_x^2 v_0 \Phi_1 \psi_s}{(v_0 - v_s)} dx \right], \end{aligned} \tag{B.8}$$

where

$$P \int_{x_1}^{x_2} \frac{\partial_x^2 v_0 \psi_s^2}{(v_0 - v_s)^2} dx = \lim_{\delta \rightarrow 0} \left[\int_{x_1}^{x_s - \delta} \frac{\partial_x^2 v_0 \psi_s^2}{(v_0 - v_s)^2} dx + \int_{x_s + \delta}^{x_2} \frac{\partial_x^2 v_0 \psi_s^2}{(v_0 - v_s)^2} dx \right]$$

denotes the principal part of Cauchy. We are interested in the last integral in (B.8) which we denote by I

$$I = \lim_{c \rightarrow v_s} \int_{x_1}^{x_2} \frac{c_i}{(v_0 - c_r)^2 + c_i^2} \frac{\partial_x^2 v_0 \Phi_1 \psi_s}{(v_0 - v_s)} dx.$$

We have for $\delta > 0$ small enough

$$\begin{aligned} I &\sim \lim_{c \rightarrow v_s} \int_{x_s - \delta}^{x_s + \delta} \frac{Im(c)}{(v_0 - Re(c))^2 + Im(c)^2} \frac{\partial_x^2 v_0 \Phi_1 \psi_s}{(v_0 - v_s)} dx \\ &\sim \lim_{c \rightarrow v_s} \int_{x_s - \delta}^{x_s + \delta} \frac{Im(c)}{(v_0 - Re(c))^2 + Im(c)^2} \frac{\frac{\partial_x^2 v_0 - 0}{x - x_s} \Phi_1 \psi_s}{\frac{v_0 - v_s}{x - x_s}} dx \\ &\sim \frac{M}{L} \lim_{c \rightarrow v_s} \int_{x_s - \delta}^{x_s + \delta} \frac{Im(c)}{(v_0 - Re(c))^2 + Im(c)^2} dx \end{aligned} \tag{B.9}$$

with $L = \partial_x v_0|_{x=x_s}$ and $M = \partial_x^3 v_0 \psi_s^2|_{x=x_s}$. Expanding $v_0(x)$ around $x = x_s$, leads to

$$v_0 = v_s + L(x - x_s) + \mathcal{O}(x - x_s)^4$$

and I becomes

$$I \sim \text{sign}(L) \frac{M}{L} \lim_{c \rightarrow v_s} \left[\arctan \left(\frac{L\delta - \text{Re}(c) + v_s}{\text{Im}(c)} \right) + \frac{1}{L} \arctan \left(\frac{L\delta + \text{Re}(c) - v_s}{\text{Im}(c)} \right) \right].$$

Since $L \neq 0$ and $\delta > 0$, it comes $I \sim \pi \text{sign}(L) M / L^2$ and (B.8) becomes

$$\frac{dc}{dk_y^2} \Big|_{k_y=k_{ys}} = - \int_{x_1}^{x_2} \psi_s^2 dx \Big/ \left[P \int_{x_1}^{x_2} \frac{\partial_x^2 v_0 \cdot \psi_s^2}{(v_0 - v_s)^2} dx + \pi \text{sign}(L) \frac{M}{L^2} \right]. \tag{B.10}$$

It is now possible to compute $\text{Im}(c)$ near the neutral stable solution using the following Taylor expansion

$$c \equiv \frac{\omega}{k_y} = c|_{k_y=k_{ys}} + (k_y - k_{ys}) \left(\frac{dc}{dk_y} \right)_{k_y=k_{ys}} + \mathcal{O}(k_y - k_{ys})^2. \tag{B.11}$$

As an example, we consider the following conditions

$$\rho_0(x) = \sin x, v_0(x) = \cos(k_0 x), \quad x_1 = 0, \quad x_2 = 2\pi, \quad k_0 = 1,$$

so that (B.3) becomes

$$(\cos x - c)(\partial_x^2 - k_y^2)\Phi_1 + \Phi_1 \cos x = 0, \quad 0 \leq x \leq 2\pi. \tag{B.12}$$

The inflexion points for v_0 are $x_s = \pi/2$ and $x_s = 3\pi/2$. To find the neutral stable solution, we consider (B.5) with $v_s = v_0(x_s) = \cos x_s = 0$ to get

$$\cos x (\partial_x^2 \Phi_s + (1 - k_{ys}^2)\Phi_s) = 0, \quad 0 \leq x \leq 2\pi,$$

or

$$\partial_x^2 \Phi_s + (1 - k_{ys}^2)\psi_s = 0, \quad 0 \leq x \leq 2\pi, \tag{B.13}$$

with periodic boundary conditions. In this case, there exists an antisymmetric solution $\psi_s = \sin nx$ and a symmetric solution $\psi_s = \cos nx$ whereas $k_{ys} = \sqrt{1 - n^2}$ for $n < (x_2 - x_1) / 2\pi$. In the present case, since $x_2 - x_1 = 2\pi$, the neutral stable solution exists only for $n = 0$. Hence,

$$\psi_s = 1, \quad k_{ys} = 1. \tag{B.14}$$

It can be proven that the instability ($\text{Im}(c) > 0$) exists (see [3]) for $k_y < k_{ys} = 1$ and the stability ($\text{Im}(c) = 0$) exists for $k_y \geq 0$. We can now compute the real and imaginary part of $\omega = k_y c$ using (B.10), (B.11)

$$c_r = \Re(\omega) / k_y = 0, \quad c_i = \Im(\omega) / k_y = 2(k_{ys} - k_y). \tag{B.15}$$

In [21], the initial condition for (4.1)-(4.2) is

$$n(x, y, t = 0) = n_0(x) + \varepsilon n_1(x) \cos(k_y y), \tag{B.16}$$

where n_1 satisfies the linearized Poisson equation: $n_1(x) = -\partial_y^2 \psi_s + k_y^2 \psi_s = k_y^2 = cste$.

B.2 Discrete computation

Starting from Eq. (B.3) with $v_0(x) = \cos x$, it is possible to apply finite difference operators for the approximation of the x -derivatives of Φ_1 . This leads to a matricial system of the form

$$A\Phi_1 = cB\Phi_1,$$

where A and B are two matrices of size N_x . Then, eigenvalues of $B^{-1}A$ can be found. Looking for the eigenvalue which has the larger imaginary part gives the instability growth rate. One of the advantage of this approach compared to the previous one is it can be used for arbitrarily value of k whereas the analytical computations are based on Taylor expansions which are valid locally.

References

- [1] A. Brizard, J. Plasma Phys. 41, p. 541, (1989).
- [2] N. Crouseilles, M. Mehrenberger, E. Sonnendrücker, Conservative Semi-Lagrangian schemes for Vlasov equations, J. Comput. Phys. 229, pp 1927-1953, (2010).
- [3] P. G. Drazin, L. N. Howard, In Advances in Applied Mechanics, (Ed. G. Kuerti), Academic Press. New York, (1966).
- [4] M. Fivaz, S. Brunner, G. de Ridder, O. Sauter, T.M. Tran, J. Vaclavik, L. Villard, K. Appert, Finite element approach to global gyrokinetic Particle-In-Cell simulations using magnetic coordinates, Comput. Phys. Comm. 111, pp. 27-47, (1998).
- [5] F. Huot, A. Ghizzo, P. Bertrand, E. Sonnendrücker Instability of the time splitting scheme for the one-dimensional and relativistic Vlasov-Maxwell system, J. Comput. Phys. 185, pp. 512-531, (2003).
- [6] M. L. Glasser, E. Montaldi, Some integrals involving Bessel functions, arXiv9307213v1, (1993).
- [7] V. Grandgirard, M. Brunetti, P. Bertrand, N. Besse, X. Garbet, P. Ghendrih, G. Manfredi, Y. Sarrazin, O. Sauter, E. Sonnendrücker, J. Vaclavik, L. Villard, A drift-kinetic semi-Lagrangian 4D code for ion turbulence simulation, J. Comput. Phys. 217, pp. 395-423, (2006).
- [8] R. M. Gray, Toeplitz and circulant matrices: a review, Now Publishers Inc, Boston-Delft, 2005.
- [9] K. Gustafson, D. del Castillo-Negrete, W. Dorland, Finite Larmor radius effects on non-diffusive tracer transport in a zonal flow, <http://arxiv.org/pdf/0807.4516>.
- [10] T.S. Hahm, Nonlinear Gyrokinetic Equations for Tokamaks Microturbulence, Phys. Fluids 31, p. 2670, (1988).
- [11] F.R. Hansen, G. Knorr, J.P. Lynov, H.L. Pécseli, J.J. Rasmussen, A numerical plasma simulation including finite Larmor radius effects to arbitrary order, Plasmas Phys. and Control. Fusion 31, pp. 173-183, (1989).
- [12] R. Hatzky, A. Koenies, A. Mishchenko, Electromagnetic gyrokinetic PIC simulation with an adjustable control variates method, J. Comput. Phys. 225, pp. 568-590, (2007).
- [13] Y. Idomura, M. Ida, T. Kano, N. Aiba, S. Tokuda, Conservative global gyrokinetic toroidal full- f five-dimensional Vlasov simulation, Comput. Phys. Comm. 179, pp. 391-403, (2008).
- [14] B. Krane, H.L. Pécseli, K. Rypdal, J. Trulsen, Finite Larmor radius effects in two-dimensional electrostatic plasma turbulence, J. de Physique IV 5, Colloque C6, suppl. J. Physique II, (1995).
- [15] G. Knorr, H. L. Pécseli, Asymptotic state of the finite-Larmor-radius guiding-centre plasma, J. Plasma Physics 41, pp. 157-170, (1989).
- [16] W. W. Lee, A gyrokinetic approach in particle simulation, Phys. Fluids 26, p. 556, (1983).

- [17] Z. Lin, W. W. Lee, Method for solving the gyrokinetic Poisson equation in general geometry, *Phys. Rev. E* 52, p. 5646, (1995).
- [18] A. Mishchenko, A. Koenies, R. Hatzky, Particle simulations with a generalized gyrokinetic solver, *Phys. Plasmas* 12, 062305, (2005).
- [19] Y. Sarazin, V. Grandgirard, E. Fleurance, X. Garbet, P. Ghendrih, P. Bertrand, G. Depret, Kinetic features of interchange turbulence, *Plasma Phys. Control. Fusion* 47, pp.1817-1839, (2005).
- [20] B. D. Scott, The gyrokinetic equation, internal notes.
- [21] M. Shoucri, A two-level implicit scheme for the numerical solution of the linearized vorticity equation, *Int. J. Numer. Meth. Eng.* 17, 1525 (1981).
- [22] M. Shoucri, J. Lebas, G. Knorr, P. Bertrand, A. Ghizzo, G. Manfredi, I. Christopher, Effect of viscous dissipation on the generation of shear flow at a plasma edge in the finite gyro-radius guiding-center, *Physica Scripta*, 1996.
- [23] E. Sonnendrücker, Modèles Cinétiques pour la Fusion, Université de Strasbourg, France, Cours Master 2 (2008).
- [24] E. Sonnendrücker, J. Roche, P. Bertrand, A. Ghizzo, The Semi-Lagrangian Method for the Numerical Resolution of the Vlasov Equation, *J. Comput. Phys.* 149, 201-220 (1999).
- [25] M. Zerroukat, N. Wood, A. Staniforth, The Parabolic Spline Method (PSM) for conservative transport problems *Internat. J. Numer. Meth. in Fluids* 51, pp. 1297-1318, (2006).